Molecular Therapy
Nucleic Acids
Brief Report

Extracellular vesicle transfer of lncRNA H19 splice variants to cardiac cells

Andreia Vilaça,[1,2,4,5] Carlos Jesus,[1,3] Miguel Lino,[1,2,3] Danika Hayman,[6] Costanza Emanueli,[6] Cesare M. Terracciano,[6] Hugo Fernandes,[1,3,7,8] Leon J. de Windt,[4,8] and Lino Ferreira[1,3,8]

[1]Center for Neuroscience and Cell Biology (CNC), Centre for Innovative Biomedicine and Biotechnology (CIBB), University of Coimbra, Coimbra, Portugal; [2]Institute of Interdisciplinary Research (IIIUC), University of Coimbra, Coimbra, Portugal; [3]Faculty of Medicine (FMUC), University of Coimbra, Coimbra, Portugal; [4]Department of Cardiology, Faculty of Health, Medicine, and Life Sciences, Maastricht University, Maastricht, the Netherlands; [5]PhD Program in Experimental Biology and Biomedicine, Institute for Interdisciplinary Research (IIIUC), University of Coimbra, Coimbra, Portugal; [6]Imperial College London, National Heart and Lung Institute, London, UK; [7]Multidisciplinary Institute of Ageing (MIA-Portugal), University of Coimbra, Coimbra, Portugal

The delivery of therapeutic long non-coding RNAs (lncRNA) to the heart by extracellular vesicles (EVs) is promising for heart repair. H19, a lncRNA acting as a major regulator of gene expression within the cardiovascular system, is alternatively spliced, but the loading of its different splice variants into EVs and their subsequent uptake by recipient cardiac cells remain elusive. Here, we dissected the cellular expression of H19 splice variants and their loading into EVs secreted by Wharton-Jelly mesenchymal stromal/stem cells (WJ-MSCs). We demonstrated that overexpression of the mouse H19 gene in WJ-MSCs induces the expression of H19 splice variants at different levels. Interestingly, EVs isolated from the H19-transfected WJ-MSCs (EV-H19) showed similar expression levels for all tested splice variant sets. *In vitro*, we further demonstrated that EV-H19 was taken up by cardiomyocytes, fibroblasts, and endothelial cells (ECs). Finally, analysis of EV tropism in living rat myocardial slices indicated that EVs were internalized mostly by cardiomyocytes and ECs. Collectively, our results indicated that EVs can be loaded with different lncRNA splice variants and successfully internalized by cardiac cells.

INTRODUCTION

Extracellular vesicles (EVs) are a class of small cell-secreted particles (30–1,000 nm) that mediate cell-to-cell communication by transferring RNAs and proteins incorporated during their biogenesis to target cells, ultimately modulating their function.[1,2] *In vivo* data in rodent and swine models indicate that stem cell-derived EVs can be used to restrain the post-myocardial infarction adverse cardiac remodeling and loss of cardiac function by promoting the survival of cardiac cells and angiogenesis.[3–6] The noncoding RNA cargo of EVs is considered to play a substantial role in EV bioactivity.[3,7,8] O'Brien et al. recently showed that long-noncoding RNAs (lncRNAs) can be transferred to recipient cells via EVs.[9] lncRNAs constitute a highly diverse group of transcripts, generally characterized as RNAs longer than 200 nt that do not encode functional proteins.[10] Their biogenesis, which has been shown to be distinct from that of mRNAs,[11] has been linked to their specific subcellular location and function.[10] Similarly to protein-encoding genes, through alternative splicing, lncRNA genes can generate several splice variants with distinct tertiary structures, new open reading frames for small peptides or the ability to produce different circular RNAs,[12] giving rise to transcripts with diverse functions.[13,14] Since lncRNAs have important regulatory roles, the altered expression of specific splice variants should be taken into account when designing therapeutic interventions.[15]

lncRNA H19, described for the first time as a non-protein-coding RNA molecule in 1990,[16] is one of the most studied lncRNAs in the cardiovascular arena. Importantly, EVs enriched in H19 have been used as a potential therapeutic platform to regenerate the heart after myocardial infarction.[17] Unfortunately, it is relatively unknown (1) which H19 splice variants are encapsulated in EVs, (2) which H19 splice variants are delivered by EVs in different cardiac cells, and (3) what is the tropism of H19-enriched EVs for cardiac cells. The current report attempts to address these questions.

RESULTS

To understand the impact of H19 splice variants in the cardiac context, we first analyzed the mouse H19 locus (located on chromosome 7 in the reverse strand) and identified the 16 annotated splice variants (Mouse Genome Reference GRCm39; GenBank: CM001000.3) (Figure 1A). We then designed primers to amplify different sets of H19 splice variants (Figure 1B). H19 is considered conserved among humans and rodents.[18] It has been widely described that H19 expression in the mouse heart steeply diminishes throughout life;[18] however, the influence of each splice variant has not been addressed before. Our results showed that, compared to the embryonic heart, the expression of all tested splice variants was lower in 8-week adult mouse hearts (Figure 1C), though the decrease observed differed among the different sets of splice variants. The higher downregulation through development was seen for sets B

Received 1 November 2023; accepted 29 May 2024;
https://doi.org/10.1016/j.omtn.2024.102233.

[8]These authors contributed equally

Correspondence: Lino Ferreira, Center for Neuroscience and Cell Biology, Centre for Innovative Biomedicine and Biotechnology, University of Coimbra, Coimbra, Portugal.
E-mail: lino.ferreira@uc.pt

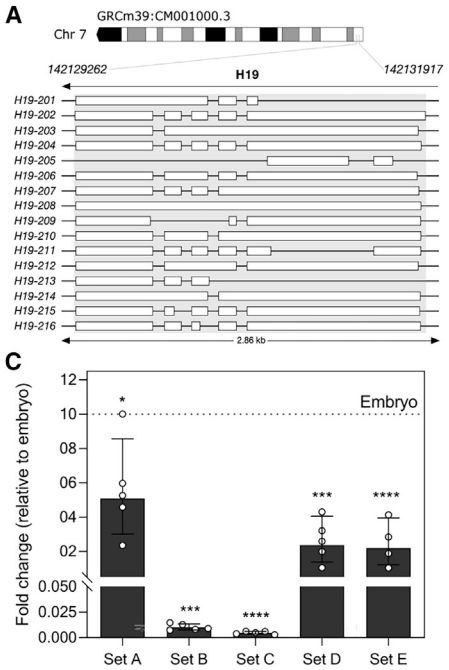

B

H19 Isoforms	Set A	Set B	Set C	Set D	Set E
201	X				
202		X	X		
203		X		X	X
204		X	X		
205					
206		X		X	X
207		X	X		
208	X	X			X
209		X			
210		X			X
211		X	X		
212		X		X	X
213			X		
214	X	X			X
215		X			
216		X	X		

Figure 1. lncRNA H19 has 16 splice variants, and their expression decreases through development

(A) The mouse H19 gene is located in the reverse strand of chromosome 7. Sixteen splice variants have been annotated. Mouse genome reference: GRCm39 (GenBank:CM001000.3). (B) The splice variants detected by the 5 designed primer pairs. (C) RT-qPCR analysis of different H19 splice variant sets present in hearts from embryo or adult mice, showing downregulation of all tested splice variants sets in adult hearts. Error bars represent geometric mean and geometric SD; $^{*}p \leq 0{,}05$, $^{***}p \leq 0.001$, $^{****}p \leq 0.0001$.

and C. Sets D and E were decreased to a lower extent in the adult mouse heart, while set A suffers the least downregulation. Overall, regardless of the splice variant set, H19 expression decreased during development, which might at least partially explain the decreased regeneration capacity of the adult heart.

Due to its large size,[19] it is not feasible to chemically synthetize H19, and therefore earlier studies have mostly relied on the use of viral vectors to overexpress H19 in target cells. Here, we analyzed the expression of H19 splice variants following the overexpression of H19 in Wharton-Jelly mesenchymal stromal/stem cells (WJ-MSCs) and their subsequent sorting into EVs. MSCs were used as EV donors due to their desirable immunomodulatory properties and the cardiac protective and pro-regenerative effects of the secreted EVs.[20,21] Human WJ-MSCs were transfected with mammalian expression vectors and harvested after 48 h (Figure 2A). RT-qPCR analysis of splice variant set expression demonstrated that H19 transfection significantly increased the expression of all tested H19 splice variant sets; on average, ~230–6,176 copies/ng RNA (Figure 2B). Then, EVs secreted from mock- or H19-transfected cells, hereafter referred to as EV-Entry or EV-H19, were isolated from the conditioned medium. EV characterization demonstrated that EV-Entry and EV-H19 had similar sizes (Figure 2C), concentration yield (Figure 2D), zeta potential (Figure 2E), protein concentration (Figure 2F), and purity (Figure 2G). Western blot characterization of EV lysates confirmed expression of CD9 and CD63 as well as Glyceraldehyde 3-phosphate dehydrogenase (GAPDH) and absence of calnexin, consistent with a small EV preparation from cell culture origin (Figure S1).

Splice variants may be differentially sorted into EVs at the parental cell due to specific interactions of the transcript with RNA binding proteins involved in the RNA export to EVs. To assess the presence of H19 splice variants in EVs, RT-qPCR analysis was performed on EV-Entry and EV-H19 (Figure 2H). Our results showed that all evaluated splice variant sets were present in the EVs at higher copy number (Figure 2H) per nanogram of RNA compared to their expression by the parental cells (Figure 2B). Expression of sets B and C in EV-H19 was increased to similar levels. Notably, sets A and D, which showed low expression in H19-transfected WJ-MSC, were shown to be expressed at higher levels in EVs, comparable to set B and set C, which were highly expressed in the WJ-MSCs after transfection. Strikingly, set E, which showed a low expression in H19-transfected WJ-MSCs, was detected in EV-H19 (mean of ≈12,000 copies/ng of total RNA), albeit with a lower expression compared to the other splice variant sets.

The distribution of the splice variants among the individual EVs in the sample remains elusive, and it is still unclear whether all of the isoforms are present within a single EV or whether different isoforms are loaded in specific EV subpopulations. Understanding the uptake of EVs by the recipient cells and their capacity to transfer RNAs may

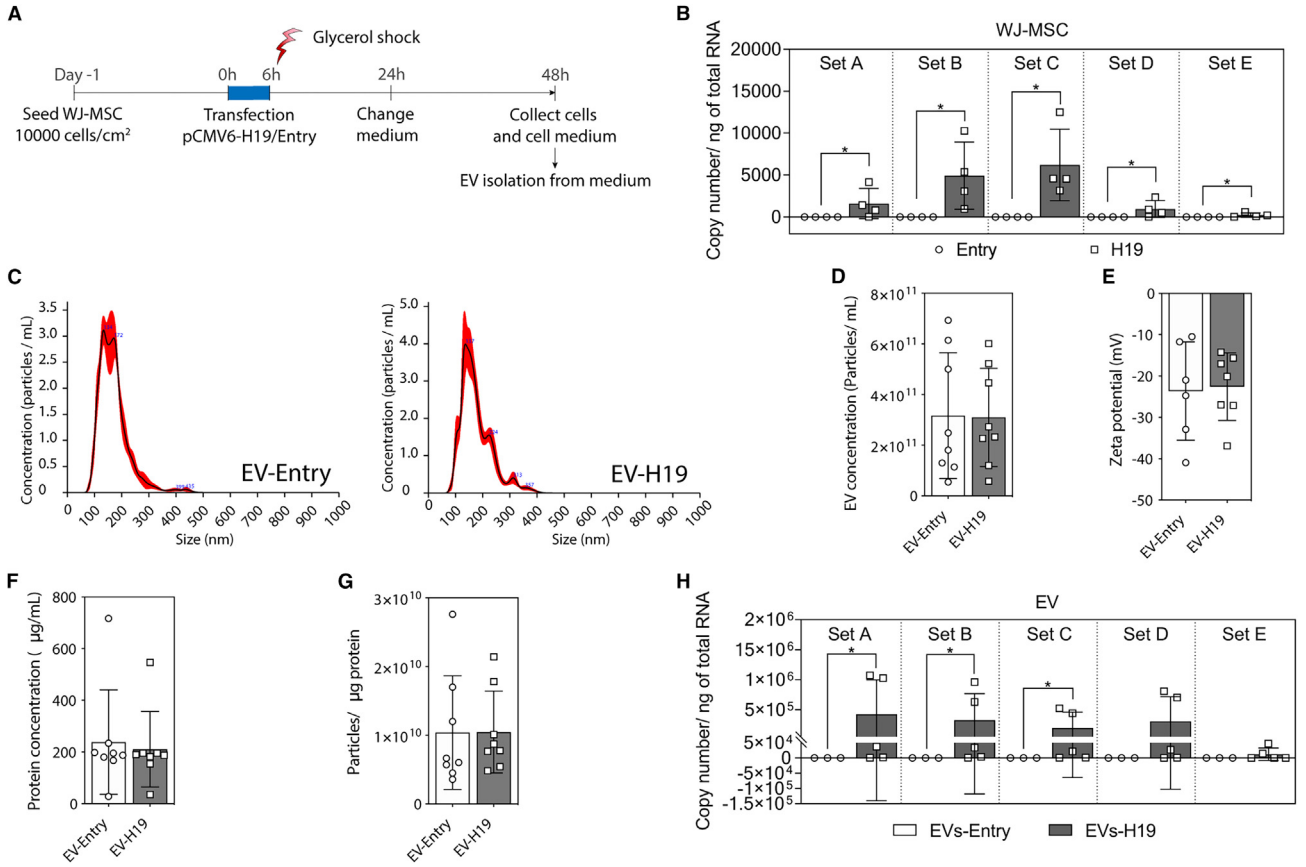

Figure 2. Transfection of plasmid DNA encoding H19 leads to the transcription of different H19 splice variants that are then packaged and released in EVs

(A) Schematic of WJ-MSC transfection with pCMV6-H19 or pCMV6-Entry, followed by EV isolation, (B) RT-qPCR analysis of different H19 splice variants expressed by WJ-MSC 48 h after transfection, demonstrating that all tested splice variants sets are expressed in the cells. (C–G) EV-Entry and EV-H19 characterization demonstrating similar (C) size distribution, (D) particle concentration after isolation, (E) zeta potential, (F) protein concentration, and (G) particles/µg protein. (H) RT-qPCR analysis of different H19 splice variants sets present in the EVs isolated from transfected WJ-MSCs, demonstrating that all tested splice variants sets are present in the EVs, albeit at different ratios than the ones found in the parental cells. Error bars represent mean ± SD; $^{*}p \leq 0.05$.

provide further insights into the distribution of the different splice variants in the EV sample. To evaluate EV uptake by the major cardiac cell types, we treated neonatal mouse cardiomyocytes (Figure 3A), mouse neonatal cardiac fibroblasts (Figure 3C), and mouse aortic endothelial cells (MAECs) (Figure 3E) with 3 $\times 10^{10}$ part/mL WJ-MSC PKH67-labeled EVs for 4 h. Confocal imaging suggested that EVs were internalized by all cardiac cell types evaluated. Moreover, our results showed that fibroblasts internalized higher levels of EVs (87.6% ± 11.2%) than cardiomyocytes (51.2% ± 8.3%) and MAECs (59.8% ± 22.3%) (Figure S2). Interestingly, neonatal mouse cardiomyocytes showed a larger EV focus size compared to both cardiac fibroblasts and MAECs (Figures 3 and S2C). We further compared the EV internalization level of adult mouse cardiomyocytes (16.6% ± 16.1%), which was found to be lower and more variable than in neonatal mouse cardiomyocytes (Figures S2D–S2F).

Next, to evaluate RNA transfer from the EVs to the recipient cells, we treated neonatal mouse cardiomyocytes (Figure 3B), mouse neonatal cardiac fibroblasts (Figure 3D), and MAECs (Figure 3F) with EV-Entry or EV-H19 for 4 h and assessed the H19 splice variant copy number by RT-qPCR. Preliminary results obtained by us indicate that H19 transcripts transported within the EVs were functional upon delivery to the recipient cells (Figure S3). Cardiomyocytes (Figure 3B) were shown to express very low levels of sets A, B, and D and higher expression of set C. Set E was not detected in cardiomyocytes. Upon treatment with EV-H19, there was a significant increase in the expression of set A, B, and D, demonstrating the transfer of RNA from the EVs to cardiomyocytes within 4 h. An increase in set E was also detected in EV-H19-treated cardiomyocytes, although this was not statistically significant. Interestingly, expression of set C, which was already highly expressed in cardiomyocytes, was not affected by EV-H19 uptake. Fibroblasts (Figure 3D) showed a low expression of sets B and D and higher expression of set C. Contrarily, set A and E were not detected in fibroblasts. Treatment with EV-H19 induced a statistically significant increase in the expression of sets A, B, and D. Expression of sets E and C was also increased by EV-H19

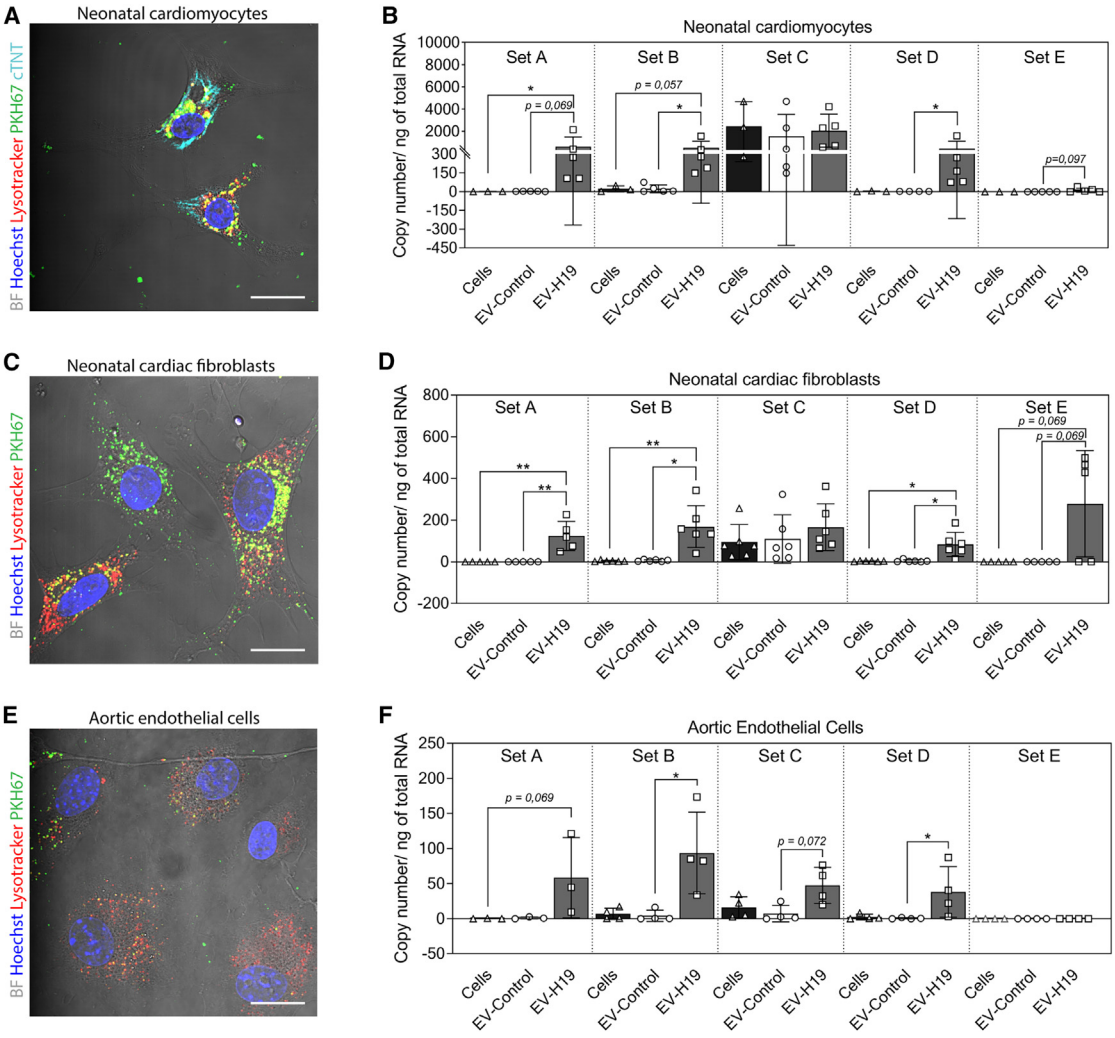

Figure 3. CMs, fibroblasts, and ECs quickly take up EVs and increase the expression of most of the H19 splice variants upon treatment with EV-H19

(A) Representative confocal image depicting EV internalization by neonatal mouse CMs. Scale bar, 20 μm. (B) RT-qPCR analysis of different H19 splice variants expressed by CMs after 4-h incubation with EV-Entry or EV-H19. (C) Representative confocal image depicting EV internalization by neonatal mouse cardiac fibroblasts. Scale bar, 20 μm. (D) RT-qPCR analysis of different H19 splice variants expressed by fibroblasts after 4-h incubation with EV-Entry or EV-H19. (E) Representative confocal image depicting EV internalization by aortic ECs. Scale bar, 20 μm. (F) RT-qPCR analysis of different H19 splice variants expressed by ECs after 4-h incubation with EV-Entry or EV-H19. Error bars represent mean ± SD; $^{*}p \leq 0.05$, $^{**}p \leq 0.01$, $^{***}p \leq 0.001$.

treatment, although the difference was not statistically significant. ECs (Figure 3F) express very low amounts of sets A, B, and D, whereas the expression of set C was slightly higher. Similar to cardiomyocytes and fibroblasts, set E expression was undetected in ECs. Treating ECs with EV-H19 for 4 h induced a statistically significant increase in the expression of sets B and D, and, although not significant, an increase in the expression of sets A and C was also observed. Intriguingly, set E expression was not altered by EV-H19 uptake remaining undetected after EV-H19 treatment. Notably, compared to cardiomyocytes and fibroblasts, the limited increase in the expression of the H19 splice variants in ECs is in line with the lower internalization profile observed with native EVs labeled with PKH67 (Figure 3E). Last, we compared the expression of EV-H19 from WJ-MSCs with direct transfection of the H19 plasmid in ECs (recipient cells). Our results show higher expression of the splice variants in EV-H19 than in cells transfected with the H19 plasmid (see Figures 2H vs. S4).

EV uptake in different cardiac cell types has been demonstrated *in vitro*, but uptake in more complex models has not been fully explored. To understand the natural tropism of EVs in a more complex cardiac setting while avoiding the influence of systemic interactions, we made use of cardiac slices.[22] The organotypic heart slice preparations are thin (<400 μm) enough to ensure sufficient oxygen supply and diffusion of metabolic waste while retaining the native cellular composition, architecture, and physiology of the heart *in vitro*. Hypoxia-reoxygenation was induced in these organotypic

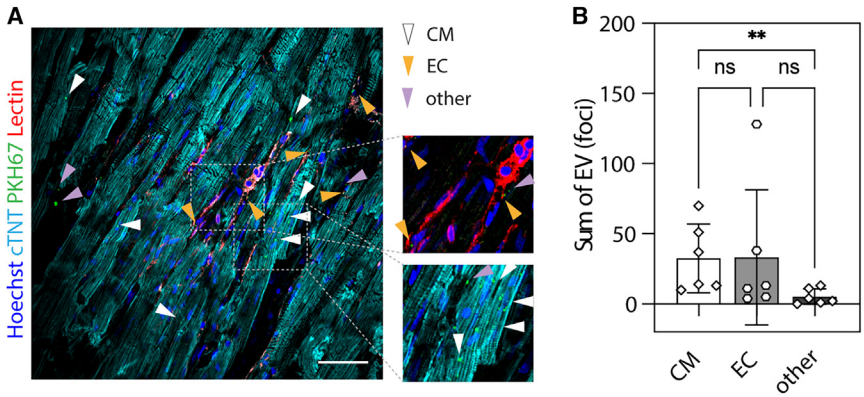

Figure 4. EVs are internalized by CMs and ECs both throughout the cardiac slice

(A) Representative confocal images of cardiac slices incubated for 24 h with PKH67-labeled EVs. Scale bar, 50 μm. White arrows indicate EVs taken up by a cardiomyocyte (CM), yellow arrows indicate EVs internalized by endothelial cells (ECs), and violet arrows indicate EVs internalized by other non-labeled cells (other). The imaged is magnified to allow the identification of EV foci in EC (top) and in CMs (bottom). (B) Sum of the EV foci that colocalize with a CM, with an EC, or with none of the prior cells (other), quantified in three z stacks of eight "z" for each independent cardiac slice (*n*), after 24-h incubation, demonstrating EV internalization by CMs, ECs, and other cells. Error bars represent mean ± SD; $^{**}p \leq 0.01$.

cultures (materials and methods) before exposure to EVs. Rat cardiac slices were treated with 1×10^8 native WJ-MSC PKH67-labelled EVs for 24 h. Confocal imaging analysis of the number of EV foci colocalizing with cardiomyocytes ($PKH67^+$/cardiac troponin T^+) or ECs ($PKH67^+$/isolectin $B4^+$) demonstrated that the majority of EVs were taken up and processed, both by cardiomyocytes and ECs but also other cell types (Figures 4A and 4B) (cardiomyocytes [CMs]: 32.50 ± 24.48; ECs: 33.17 ± 48.08; other: 5.17 ± 5.50; values represent the sum of EV foci per cell type in all images acquired for one cardiac slice sample). Of note, analysis of EV distribution (Figure S5) in "z" within the cardiac slice 24 h post treatment showed that the PKH67 signal was observed not only at the surface but also in deeper cell layers both for CMs and ECs. Since CMs and ECs were not presented in similar proportions in the slices, accurate analysis of tropism might require information on the cellular composition of the rat heart. Although it is commonly accepted that CMs represent 30% of the heart cells,[23] initial studies of the rat heart have shown that CMs account for around 75% of the volume of the heart, while ECs only take up 3% of the volume.[24] Here we hypothesize that the higher surface-area-to-volume ratio of the CMs would provide increased opportunity for interaction and internalization of EVs, similarly to what was seen for nanoparticles,[25] rather than specific tropism to CMs. Remarkably, the EV foci quantified within CMs and ECs were similar, and each represented around 50% of the total quantified EV foci, suggesting a preferential uptake by ECs, since they are expected to only represent 3% of the volume of the heart. However, it is important to note that a single CMs could span more than one "z." This is difficult to account for in the analysis due to multinucleation of CMs, which impedes accurate distinction and quantification of a single CM.

DISCUSSION

Here, we provide evidence that EVs can be loaded with different H19 splice variants and successfully delivered to different cardiac cell types both in 2D cultures as well as in more physiologically relevant models (*ex vivo* cardiac slices). Our results suggest that, upon transcription of H19 splice variants in the EV-secreting cells, different variants were sorted to EVs. Currently, literature on the mechanisms governing lncRNA packaging and sorting to EVs is scarce. The protein heterogeneous nuclear ribonucleoprotein A2B1 (hnRNPA2B1) has been the only one already described to bind to[26] and mediate H19 packaging and sorting to EVs,[27] although the exact mechanism has not been dissected.

Our *in vitro* results further show that fibroblasts internalized more EVs than CMs and MAECs. The larger EV focus size in CMs than in other cardiac cells suggest higher intracellular accumulation of EVs, likely in the endolysosomal compartment, but this requires further testing in the future. While our findings align with previous research,[28] other EV internalization studies have demonstrated opposite profiles, with ECs being the cell type that takes up the most EVs.[17] This is likely due to differences in the source of EVs, EV dose, and treatment duration as well as inherent differences in the cell models used to test the internalization. Interestingly, our studies of EVs with cardiac slices suggest that ECs are the cardiac cells that internalize more EVs. At the moment, the reasons for the differences obtained between isolated cells and cardiac slices are not clear; however, it shows the importance of having different cellular and *ex vivo* models to fully investigate the interaction of EVs with tissues/organs.

Although it is not clear whether lncRNA packing into EVs is done in a homogeneous (each EV contains similar amounts of a given transcript) or in a heterogeneous way (transcripts are distributed differently within each EV), the differences observed in the internalization profile of each cell type hint toward the latter process being the most likely. If heterogeneous distribution of the transcripts among the individual EVs would take place, that would, for instance, explain why set E is not detected in ECs, while it was found in EVs and then in fibroblasts.

Further research into the relevance of each splice variant in the context of cardiac disease and how to manipulate their expression in EVs could improve therapeutic potential by selectively delivering the required splice variants to the target cells.

MATERIALS AND METHODS

Due to space limitations, the Materials and methods can be found online in the supplemental information.

DATA AND CODE AVAILABILITY

Data that support the findings of this study are available from the corresponding author upon request.

SUPPLEMENTAL INFORMATION

Supplemental information can be found online at https://doi.org/10.1016/j.omtn.2024.102233.

ACKNOWLEDGMENTS

The authors would like to acknowledge Crioestaminal (www.crioestaminal.pt) for providing samples and other helpful information and Dr. Yingqun Huang for providing the lncRNA H19 plasmid. The authors would further like to acknowledge funding by the FCT PhD Studentships (SFRH/BD/119187/2016 and SFRH/BD/144092/2019), Programa Operacional Competividade e Internacionalização (POCI) na sua componente FEDER e pelo orçamento da Fundação para a Ciência e a Tecnologia na sua componente OE (Project 2022.03308.PTDC), EC projects RESETaging (ref. 952266) and REBORN (ref. 101091852), and PRR project HfPT-Health from Portugal (ref. 02/C05-i01.01/2022.PC644937233-00000047). L.J.d.W. acknowledges support from the Dutch Cardiovascular Alliance (ARENA-PRIME). L.J.d.W. was further supported by a VICI award (918-156-47) from the Dutch Research Council, Marie Sklodowska-Curie grant agreement 813716 (TRAIN-HEART), and a PPP allowance made available by Health∼Holland, Top Sector Life Sciences & Health, under agreement LSHM21068 to stimulate public-private partnerships.

AUTHOR CONTRIBUTIONS

A.V., C.J., M.L., and D.H. conducted the experiments. A.V., C.J., H.F., L.J.d.W., and L.F. designed the experiments. A.V., C.J., M.L., D.H., C.E., C.M.T., H.F., L.J.d.W., and L.F. analyzed the experiments. A.V. and C.J. analyzed the data. A.V., C.J., H.F., L.J.d.W., and L.F. wrote the paper.

DECLARATION OF INTERESTS

The authors declare no competing interests.

REFERENCES

1. Vilaca, A., de Windt, L.J., Fernandes, H., and Ferreira, L. (2023). Strategies and challenges for non-viral delivery of non-coding RNAs to the heart. Trends Mol. Med. *29*, 70–91.
2. de Abreu, R.C., Fernandes, H., da Costa Martins, P.A., Sahoo, S., Emanueli, C., and Ferreira, L. (2020). Native and bioengineered extracellular vesicles for cardiovascular therapeutics. Nat. Rev. Cardiol. *17*, 685–697.
3. Agarwal, U., George, A., Bhutani, S., Ghosh-Choudhary, S., Maxwell, J.T., Brown, M.E., Mehta, Y., Platt, M.O., Liang, Y., Sahoo, S., et al. (2017). Experimental, Systems, and Computational Approaches to Understanding the MicroRNA-Mediated Reparative Potential of Cardiac Progenitor Cell-Derived Exosomes From Pediatric Patients. Circ. Res. *120*, 701–712.
4. Gallet, R., Dawkins, J., Valle, J., Simsolo, E., de Couto, G., Middleton, R., Tseliou, E., Luthringer, D., Kreke, M., Smith, R.R., et al. (2017). Exosomes secreted by cardiosphere-derived cells reduce scarring, attenuate adverse remodelling, and improve function in acute and chronic porcine myocardial infarction. Eur. Heart J. *38*, 201–211.
5. Zhu, L.P., Tian, T., Wang, J.Y., He, J.N., Chen, T., Pan, M., Xu, L., Zhang, H.X., Qiu, X.T., Li, C.C., et al. (2018). Hypoxia-elicited mesenchymal stem cell-derived exosomes facilitates cardiac repair through miR-125b-mediated prevention of cell death in myocardial infarction. Theranostics *8*, 6163–6177.
6. Barile, L., Lionetti, V., Cervio, E., Matteucci, M., Gherghiceanu, M., Popescu, L.M., Torre, T., Siclari, F., Moccetti, T., and Vassalli, G. (2014). Extracellular vesicles from human cardiac progenitor cells inhibit cardiomyocyte apoptosis and improve cardiac function after myocardial infarction. Cardiovasc. Res. *103*, 530–541.
7. Cambier, L., de Couto, G., Ibrahim, A., Echavez, A.K., Valle, J., Liu, W., Kreke, M., Smith, R.R., Marbán, L., and Marbán, E. (2017). Y RNA fragment in extracellular vesicles confers cardioprotection via modulation of IL-10 expression and secretion. EMBO Mol. Med. *9*, 337–352.
8. Gollmann-Tepekoylu, C., Polzl, L., Graber, M., Hirsch, J., Nagele, F., Lobenwein, D., Hess, M.W., Blumer, M.J., Kirchmair, E., Zipperle, J., et al. (2020). miR-19a-3p containing exosomes improve function of ischaemic myocardium upon shock wave therapy. Cardiovasc. Res. *116*, 1226–1236.
9. O'Brien, K., Breyne, K., Ughetto, S., Laurent, L.C., and Breakefield, X.O. (2020). RNA delivery by extracellular vesicles in mammalian cells and its applications. Nat. Rev. Mol. Cell Biol. *21*, 585–606.
10. Statello, L., Guo, C.J., Chen, L.L., and Huarte, M. (2021). Gene regulation by long non-coding RNAs and its biological functions. Nat. Rev. Mol. Cell Biol. *22*, 96–118.
11. Quinn, J.J., and Chang, H.Y. (2016). Unique features of long non-coding RNA biogenesis and function. Nat. Rev. Genet. *17*, 47–62.
12. Aznaourova, M., Schmerer, N., Schmeck, B., and Schulte, L.N. (2020). Disease-Causing Mutations and Rearrangements in Long Non-coding RNA Gene Loci. Front. Genet. *11*, 527484.
13. Li, X., He, X., Wang, H., Li, M., Huang, S., Chen, G., Jing, Y., Wang, S., Chen, Y., Liao, W., et al. (2018). Loss of AZIN2 splice variant facilitates endogenous cardiac regeneration. Cardiovasc. Res. *114*, 1642–1655.
14. Cho, H., Li, Y., Archacki, S., Wang, F., Yu, G., Chakrabarti, S., Guo, Y., Chen, Q., and Wang, Q.K. (2020). Splice variants of lncRNA RNA ANRIL exert opposing effects on endothelial cell activities associated with coronary artery disease. RNA Biol. *17*, 1391–1401.
15. Uchida, S., and Dimmeler, S. (2015). Long noncoding RNAs in cardiovascular diseases. Circ. Res. *116*, 737–750.
16. Brannan, C.I., Dees, E.C., Ingram, R.S., and Tilghman, S.M. (1990). The product of the H19 gene may function as an RNA. Mol. Cell Biol. *10*, 28–36.
17. Huang, P., Wang, L., Li, Q., Tian, X., Xu, J., Xu, J., Xiong, Y., Chen, G., Qian, H., Jin, C., et al. (2020). Atorvastatin enhances the therapeutic efficacy of mesenchymal stem cells-derived exosomes in acute myocardial infarction via up-regulating long non-coding RNA H19. Cardiovasc. Res. *116*, 353–367.
18. Viereck, J., Bührke, A., Foinquinos, A., Chatterjee, S., Kleeberger, J.A., Xiao, K., Janssen-Peters, H., Batkai, S., Ramanujam, D., Kraft, T., et al. (2020). Targeting muscle-enriched long non-coding RNA H19 reverses pathological cardiac hypertrophy. Eur. Heart J. *41*, 3462–3474.
19. Baronti, L., Karlsson, H., Marušič, M., and Petzold, K. (2018). A guide to large-scale RNA sample preparation. Anal. Bioanal. Chem. *410*, 3239–3252.
20. Karbasiafshar, C., Sellke, F.W., and Abid, M.R. (2021). Mesenchymal stem cell-derived extracellular vesicles in the failing heart: past, present, and future. Am. J. Physiol. Heart Circ. Physiol. *320*, H1999–H2010.
21. Monguio-Tortajada, M., Prat-Vidal, C., Martinez-Falguera, D., Teis, A., Soler-Botija, C., Courageux, Y., Munizaga-Larroude, M., Moron-Font, M., Bayes-Genis, A., Borras, F.E., et al. (2022). Acellular cardiac scaffolds enriched with MSC-derived extracellular vesicles limit ventricular remodelling and exert local and systemic immunomodulation in a myocardial infarction porcine model. Theranostics *12*, 4656–4670.
22. Watson, S.A., Scigliano, M., Bardi, I., Ascione, R., Terracciano, C.M., and Perbellini, F. (2017). Preparation of viable adult ventricular myocardial slices from large and small mammals. Nat. Protoc. *12*, 2623–2639.

23. Marin-Sedeno, E., de Morentin, X.M., Perez-Pomares, J.M., Gomez-Cabrero, D., and Ruiz-Villalba, A. (2021). Understanding the Adult Mammalian Heart at Single-Cell RNA-Seq Resolution. Front. Cell Dev. Biol. *9*, 645276.

24. Anversa, P., Olivetti, G., Melissari, M., and Loud, A.V. (1980). Stereological measurement of cellular and subcellular hypertrophy and hyperplasia in the papillary muscle of adult rat. J. Mol. Cell. Cardiol. *12*, 781–795.

25. Khetan, J., Shahinuzzaman, M., Barua, S., and Barua, D. (2019). Quantitative Analysis of the Correlation between Cell Size and Cellular Uptake of Particles. Biophys. J. *116*, 347–359.

26. Zhang, Y., Huang, W., Yuan, Y., Li, J., Wu, J., Yu, J., He, Y., Wei, Z., and Zhang, C. (2020). Long non-coding RNA H19 promotes colorectal cancer metastasis via binding to hnRNPA2B1. J. Exp. Clin. Cancer Res. *39*, 141.

27. Lei, Y., Guo, W., Chen, B., Chen, L., Gong, J., and Li, W. (2018). Tumorreleased lncRNA H19 promotes gefitinib resistance via packaging into exosomes in nonsmall cell lung cancer. Oncol. Rep. *40*, 3438–3446.

28. Mentkowski, K.I., and Lang, J.K. (2019). Exosomes Engineered to Express a Cardiomyocyte Binding Peptide Demonstrate Improved Cardiac Retention in Vivo. Sci. Rep. *9*, 10041.